CrossMark

PPAR-γ Ameliorates Neuronal Apoptosis and Ischemic Brain Injury via Suppressing NF-κB-Driven p22phox Transcription

Jui-Sheng Wu[1] · Hsin-Da Tsai[1] · Wai-Mui Cheung[1] · Chung Y. Hsu[2] · Teng-Nan Lin[1,3,4]

Abstract Peroxisome proliferator-activated receptor-gamma (PPAR-γ), a stress-induced transcription factor, protects neurons against ischemic stroke insult by reducing oxidative stress. NADPH oxidase (NOX) activation, a major driving force in ROS generation in the setting of reoxygenation/reperfusion, constitutes an important pathogenetic mechanism of ischemic brain damage. In the present study, both transient in vitro oxygen-glucose deprivation and in vivo middle cerebral artery (MCA) occlusion-reperfusion experimental paradigms of ischemic neuronal death were used to investigate the interaction between PPAR-γ and NOX. With pharmacological (PPAR-γ antagonist GW9662), loss-of-function (PPAR-γ siRNA), and gain-of-function (Ad-PPAR-γ) approaches, we first demonstrated that 15-deoxy-$\Delta^{12,14}$-PGJ$_2$ (15d-PGJ$_2$), via selectively attenuating p22phox expression, inhibited NOX activation and the subsequent ROS generation and neuronal death in a PPAR-γ-dependent manner. Secondly, results of promoter analyses and subcellular localization studies further revealed that PPAR-γ, via inhibiting hypoxia-induced NF-κB nuclear translocation, indirectly suppressed NF-κB-driven p22phox transcription. Noteworthily, postischemic p22phox siRNA treatment not only reduced infarct volumes but also improved functional outcome. In summary, we report a novel transrepression mechanism involving PPAR-γ downregulation of p22phox expression to suppress the subsequent NOX activation, ischemic neuronal death, and brain infarct. Identification of a PPAR-γ→NF-κB→p22phox neuroprotective signaling cascade opens a new avenue for protecting the brain against ischemic insult.

Keywords Gene regulation · NADPH oxidase · Nox2 · NF-κB

✉ Teng-Nan Lin
bmltn@ibms.sinica.edu.tw

1 Institute of Biomedical Sciences, Academia Sinica, Rm 404, Taipei 11529, Taiwan, Republic of China

2 Graduate Institute of Clinical Medical Science, China Medical University, Taichung, Taiwan

3 Institute of Neuroscience, National Yang-Ming University, Taipei, Taiwan

4 Graduate Institute of Life Sciences, National Defense Medical Center, Taipei, Taiwan

Introduction

Stroke is the third leading cause of death and the leading cause of adult disability worldwide. Approximately 80 % of stroke is caused by cerebral ischemia [1, 2]. Early recanalization of occluded cerebral arteries resulting in better clinical outcome has been attributed to the replenishment of nutrients and oxygen, as well as removal of toxic metabolites, however, at the expense of reactive oxygen species (ROS) generation upon reperfusion. ROS-mediated oxidative stress appears to play a pivotal role in brain damage after ischemic stroke [3–5].

Among all the sources of ROS production in the brain, NADPH oxidase (NOX) is a major mechanism in the setting of cerebral ischemia-reperfusion [6–9]. A prominent action of NOX noted in the ischemic brain is the massive production of superoxide and hydrogen peroxide leading to ischemic neuronal death. NOX was first identified in immune cells, neutrophils/leukocytes, and later, virtually all cell types. Seven homologous members have been documented in the family: Nox1~5 and Duox1~2, which differ in their expression, structure, and function [10]. Among them, Nox2 (gp91phox or CYBB) is the first member that has been identified and the most extensively studied. In resting

state, Nox2 (the catalytic subunit) forms a heterodimer with p22phox (CYBA; the regulatory subunit) anchored in the plasma membrane. Upon stimulation, the cytosolic subunits p47phox, p67phox, p40phox, and small Rac GTPase (rac1/2) are recruited to the plasma membrane and bind to Nox2/p22phox to form active NOX holoenzyme. Similarly, Nox1, Nox3, and Nox4 also dimerize with p22phox in resting state. Nonetheless, Nox1 needs cofactors Noxa1, Noxo1, p47phox, and rac1/2 for full activation. Nox3, only observed in the inner ear, requires Noxo1 for full activation. While Nox4 is constitutively activated, no cytosolic cofactor is required. Based on messenger RNA (mRNA) levels, Nox4 is the most widely distributed NOX isoform in the vascular system. On the other hand, Nox5 forms homodimer in resting state and requires only calcium for activation. Nox5 is functionally less characterized since it is not expressed in rats and mice [6, 11, 12].

Nox2 activation led to postischemic neuronal death, microglia activation, inflammation, matrix metallopeptidases (MMPs), and BBB breakdown [13–15]. By contrast, inhibitors targeting Nox2 activity reduced brain infarct volume [15–19]. Moreover, smaller ischemic brain lesion was observed in mice lacking a functional phagocytic Nox2 [18, 20–22], p47phox [23], Nox1 [24], and Nox4 [25]. Convincingly, NOX plays a pivotal role in ischemic brain damage; however, NOX is expressed in microglia, astrocytes, endothelial cells, and to a less extent, neurons. In addition, multiple isoforms with low basal levels make it challenging in delineating the regulatory mechanism(s) of neuronal NOX following cerebral ischemia-reperfusion [26, 27].

Peroxisome proliferator-activated receptor-gamma (PPAR-γ; NR1C3) is a transcription factor which belongs to the nuclear hormone receptor superfamily located on human chromosome 3 [28, 29]. PPAR-γ agonists have been shown to attenuate ischemic brain damage by reducing oxidative stress [30–32], while PPAR-γ deletion led to bigger infarct [33, 34]. PPAR-γ accelerates the removal of excessive superoxide by increasing superoxide dismutase (SOD) transcription while reducing superoxide generation by lowering NOX levels. For instance, pioglitazone, a synthetic PPAR-γ agonist, increased SOD-1 expression and decreased NOX expression in human umbilical vein endothelial cells (HUVECs) [35] and decreased middle cerebral artery thickening in spontaneously hypertensive rats-stroke prone (SHRs-SP; [36]). 15-Deoxy-$\Delta^{12,14}$-PGJ$_2$ (15d-PGJ$_2$), an endogenous PPAR-γ agonist, decreased the basal activity of NOX, while increased the expression of SOD-1 in HUVECs [37] and p22phox level in hypoxic cerebral endothelial cells [38]. Rosiglitazone, a synthetic PPAR-γ agonist, inhibited NOX activity in hyperglycemic HUVECs by activating AMP-activated protein kinase [39] and ameliorated cardiovascular pathophysiologic features of SHRs by decreasing p22phox expression in the aorta [40]. Surprisingly, while the aforementioned studies were done in the vascular system, the link between these

two signaling events, PPAR-γ and NOX, has not been established in neurons and in the setting of cerebral ischemia-reperfusion. Although rosiglitazone has been shown to be a neuroprotectant via upregulation of SOD [33, 41], whether PPAR-γ agonism also confers anti-NOX function in ischemic neurons remains to be established.

Previously, we have established that PPAR-γ agonism reduced neuronal apoptosis and ischemic infarct [34, 42]. The neuroprotective action of PPAR-γ agonism was accompanied by reduced ROS levels [43]. In the present study, applying state-of-the-art molecular genetic techniques, we reported that PPAR-γ, via transrepressing p22phox transcription, inactivated NOX and attenuated both ROS generation and ischemic neuronal death in vitro in an oxygen-glucose deprivation (OGD) model and in vivo in a rodent stroke model.

Material and Methods

Cell Cultures and Oxygen-Glucose Deprivation Model

Primary cortical neurons were prepared from E15.5 mouse embryos and cultured in neurobasal plus B27 medium (Gibco, Grand Island, NY) containing 2 mM L-glutamine, 10 μM glutamate, 1.6 % FBS, 0.4 % HS, and penicillin/streptomycin. On day in vitro (DIV) 3, the cells were treated with 1 μM cytosine arabinoside (Ara-C) for 72 h to prevent glial proliferation and then maintained in serum-free neurobasal plus B27 medium at 37 °C in a humidified 5 % CO$_2$ incubator. Experiments were conducted on DIV 8~10 [44]. 15d-PGJ$_2$, GW9662, and apocynin (APO; Cayman, Ann Arbor, MI, USA) were added into cells either alone or in various combinations for 12 h prior to OGD treatment [45]. These PPAR-γ reagents were dissolved in DMSO (final concentration ≤0.1 %). In brief, OGD was conducted in a temperature-controlled (37±1 °C) anaerobic chamber (Model 1025, Forma Scientific, Marietta, OH, USA) containing a gas mixture of 5 % CO$_2$, 10 % H$_2$, 85 % N$_2$, and 0.02 % to 0.1 % O$_2$. Primary neurons on DIV 10 or cells grown to 70 % confluence were washed with deoxygenated glucose-free Hanks' balanced salt solution (HBSS, GIBCO-BRL) and then transferred to an anaerobic chamber for 30 min. After OGD, cells then underwent reoxygenation by being placed into oxygenated glucose-containing HBSS and returned to the normoxic 5 % CO$_2$/95 % air incubator for various times. Cell death or viability was determined by the extent of cytosolic lactate dehydrogenase (LDH) released into the medium and by the use of the cell counting kit 8 (CCK-8) (Dojindo Molecular Technologies, Kumamoto, Japan).

Flow Cytometry

Flow cytometry was employed to analyze normal MMP and apoptosis (sub-G$_0$/G$_1$) cell population [43]. For measurement

of MMP, cells were stained with the fluorescent dye JC-1 (Molecular Probes, Eugene, OR), which exhibits potential-dependent accumulation in the mitochondria. At low membrane potentials, JC-1 exists as a monomer and produces a green fluorescence (emission at 527 nm). At high membrane potentials, JC-1 forms J aggregates (emission at 590 nm) and produces a red fluorescence. Briefly, 1×10^6 cells were harvested and incubated with 1 ml of JC-1 in PBS (5 μg/ml) for 15 min at 37 °C in the dark. After centrifugation ($500 \times g$, 5 min), cells were resuspended in 0.5 ml PBS and analyzed by a fluorescence-activated cell sorter (FACS) caliber flow cytometer (BD Bioscience, San Jose, CA). For apoptosis analysis, cells were fixed in ice-cold 70 % ethanol for 30 min at 4 °C. After centrifugation, cells were resuspended and incubated in phosphate buffered saline containing 75 μg/ml RNase A and 10 μg/ml propidium iodide (PI) at 37 °C for 30 min and analyzed by FACSCalibur flow cytometer. Percent of cells with hypodiploid DNA (sub-G_0/G_1) was measured.

Western Blot Analysis

Western blot analysis of protein levels in primary neurons and brains was performed as described [38] with antibodies from Santa Cruz Biotechnology (Santa Cruz, CA, USA): p22phox (1:500), gp91phox (1:250), p67phox (1:500) and p47phox (1:500), p65 (1:1000), TFIID (1:250), α-tubulin (1:10,000), GAPDH (1:10,000), and PPAR-γ (1:500); from GeneTex (San Antonio, TX, USA): Nox4 (1:500), Nox1 (1:500), p40phox (1:500), rac1 (1:500), and rac2 (1:500); and from Cell Signaling Technology (Danvers, MA, USA): active caspase-3 (1:500), cleaved poly(ADP-ribose) polymerase 1 (PARP-1; 1:1000), IκBα (1:1000), and p-IκBα (1:1000). Protein bands were visualized by enhanced chemiluminescence system (Merck Millipore; Billerica, MA, USA). Subcellular fractions of primary neurons were prepared by using the ProteoJET Cytoplasmic and Nuclear Protein Extraction Kit (Fermentas, Burlington, ON, Canada).

Small Interference RNA Transient Transfection

Specific small interference RNA (siRNA) and scramble RNA (scRNA, control) were purchased from Ambion (Austin, TX, USA; PPAR-γ) and Dharmacon (Lafayette, CO, USA; p22phox). Lipofectamine 2000 (Invitrogen, Carlsbad, CA) was used as transfection carrier as previously described [34]. In brief, 4 μl of Lipofectamine 2000 and 20 pmol siRNA were mixed in 250 μl of Optimedium in a 24-well dish containing 2.5×10^5 primary neurons/well. At 5 h after transfection, the medium was replaced by a culture medium containing neurobasal plus B27 medium and cultured for an additional 19 h before OGD treatment. Transfection efficiency (~70 %) was evaluated by transfection of FAM-labeled siRNA (MDBio, Taipei, Taiwan,

ROC), and enhanced green fluorescent protein in primary neurons was measured by flow cytometry and fluorescence microscopy.

Preparation of Replication-Defective Recombinant Adenoviral Vectors

Viral vectors were prepared as described [34, 46]. In the replication-defective recombinant adenoviral (rAd) vector, we constructed a human phosphoglycerate kinase (PGK) promoter to drive PPAR-γ (Ad-PPAR-γ) or PGK alone (Ad-hPGK) as the control. Replication-defective rAd vectors were generated by homologous recombination and amplified in HEK293 cells. rAd stocks were prepared by CsCl gradient centrifugation and stored at −80 °C. Viral titers were determined by a plaque-assay method. HEK293 cells were infected with serially diluted viral preparations and then overlaid with low melting point agarose after infection. The number of plaques formed was counted within 2 weeks. Cells were infected with Ad-PPAR-γ 24 h before OGD.

Monitoring of H₂O₂ by Flow Cytometry and Fluorescent Microscopy

Cells adhering to the culture dish were pretreated with 30 μM 2′,7′-dichloro-dihydro-fluorescein diacetate (DCFH-DA) for 30 min and trypsinized for immediate analysis by flow cytometry and fluorescent microscopy. The esterified form of DCFH-DA permeates cell membranes before hydrolysis by intracellular esterase. The resulting compound, dichloro-dihydro-fluorescein (DCFH), reacts with H_2O_2 to produce an oxidized fluorescent compound, dichloro-fluorescein (DCF), which can be detected by flow cytometry with excitation and emission of 488 and 525–550 nm, respectively. H_2O_2 levels were calculated as geometric means by the use of CellQuest and expressed as arbitrary units [38]. Fluorescent images were obtained by the use of an Olympus microscope (Olympus IX71, Tokyo).

Determination of NADPH Oxidase Activity

A lucigenin-enhanced chemiluminescence assay for NADPH oxidase activity was as reported [38]. Primary neurons were homogenized in Krebs-Ringer phosphate buffer at pH 7.4 (120 mM NaCl, 4.8 mM KCl, 1.2 mM MgSO₄, 2.2 mM CaCl₂, 0.1 M phosphate buffer) with protease inhibitor cocktail (Sigma). Cell lysates were centrifuged at $500 \times g$ for 5 min at 4 °C and the pellet was discarded. The supernatant was stored at −70 °C. The total protein concentration was determined by a Bradford assay and adjusted to 1 mg/ml. A 100-μl protein sample including 5 μmol/l lucigenin was measured in quadruplicate with NADPH (100 μmol/l) used as a substrate

in a luminometer counter (OPTOCOMP I, MGM Instruments, Hamden, CT, USA). Data were collected at 3-min intervals to measure relative changes in NADPH oxidase activity.

Reporter Assay

p22phox reporter constructs were prepared by cloning a mouse promoter sequence into the pGL4-Luc vector (Promega, Madison, WI, USA) [38]. For cloning p22phox promoter, the 5′-flanking region of the mouse genomic sequence was synthesized by polymerase chain reaction (PCR) with the primer sequences for p1323 (−1323 to 1), F: 5′-tttctcgagcctgccttagagtctctgacctg-3′ and R: 5′-tttaagcttg caagtcctcactgatcggc-3′; p482 (−482 to 1), F: 5′-tttctcgagcg tgagagtctcctgccacct-3′ and R: 5′-tttaagcttgcaagtcctca ctgatcggc-3′; p100 (−100 to 1), F: 5′-tttctcgaggtcgatgg ggagactgtccc-3′ and R: 5′-tttaagcttgcaagtcctcactgatcggc-3′; Dp1323 (−1323 to 1), F: 5′-tttctcgagcctgccttagagtctctgacctg-3′ and R: 5′-tttaagcttgcaagtcctcactgatcggc-3′; and nested primers, F1: 5′-tttaagctttgcacactatggtcccctac-3′ and R1: 5′-tttaagcttgggacagaacaccggaacac-3′. The sequence was then cloned into pGL4 luciferase reporter.

△N-I-κBα plasmid, a degradation-resistant IκBα mutant, was a generous gift from Dr. Chou-Zen Giam, Uniformed Services University of the Health Sciences. A minimal cytomegalovirus promoter, pCMV-β-galactosidase (β-Gal) plasmid (Promega), was used as an internal control for transfection. Cells were lysed with reporter lysis buffer (Promega), and luciferase activity was then determined by mixing 50 μl cell lysates with 50 μl luciferase assay reagent [38].

Mouse N2-A neuroblastoma cells were obtained from the American Type Culture Collection for this study. In brief, 0.75 μl of Lipofectamine 2000 and 0.5 μg of DNA were mixed in 250 μl of Optimedium in a 24-well dish containing 8.3×10^4 N2-A cells/well. At 5 h after transfection, the medium was replaced by culture medium containing 10 % fetal bovine serum and cultured for an additional 43 h prior to OGD treatment. Transfection efficiency (~75 %) was evaluated by transfection of pEGFP-N1, and measurement of enhanced green fluorescent protein in cells was done by flow cytometry and examined under a fluorescence microscope.

Chromatin Immunoprecipitation Assay

Chromatin immunoprecipitation (ChIP) assay was performed as described [34, 38]. In brief, 5×10^6 primary neurons were incubated in 1 % formaldehyde for 15 min at room temperature. Glycine (0.125 M) was added for another 5 min. Cells were washed twice with ice-cold PBS, scraped, and lysed in lysis buffer (50 mM HEPES, pH 7.5, 140 mM NaCl, 1 % Triton X-100, 0.1 % Na-deoxycholate with 1× Thermo-Halt protease inhibitor) for 10 min at 4 °C. Lysates were sonicated 24 times at amplitude 50 and centrifuged at 16,200×g for

10 min at 4 °C to remove debris. An amount of 300 μg lysate of protein was used as DNA input control or incubated with the antibody anti-PPAR-γ, anti-NF-κB (p65), or nonimmune rabbit IgG (Santa Cruz Biotechnology) overnight at 4 °C. Immunoprecipitated complexes were collected by using protein G-Sepharose beads. The precipitates were extensively washed and incubated in the elution buffer (1 % SDS, 10 mM EDTA, and 50 mM Tris, pH 8.0) for 10 min at 65 °C. Cross-linking of protein-DNA complexes was reversed at 65 °C for 6 h to overnight, followed by treatment with 100 μg/ml proteinase K for 3 h at 50 °C. DNA was extracted by the use of a PCR purification kit (Qiagen, Düsseldorf, Germany) and then underwent PCR amplification with the primer sequence for PPRE, F: 5′-ccggagcagcggctact-3′ and R: 5′-acactcgacatcccccagta-3′ and NF-κB binding site, F: 5′-tcctgccaccttgtaacc-3′ and R: 5′-cagataaaggctgctccctaa-3′. Putative PPAR-γ binding sites (MA0065) with typical GGGGTCAAAGGTCA motif and putative NF-κB binding sites (M00052) with typical GGGG(X)TTTCC (X denotes any nucleotide) motif on mouse p22phox promoter region were analyzed by the use of multigenome analysis of positions and patterns of elements of regulation (MAPPER; http://bio.chip.org/mapper/mapper-main). The primers for amplifying PPRE-containing region on 14-3-3ε promoter are F: 5′-ctcgagatctctgttggcatattttttgtctattttac-3′ and R: 5′-aaaaagcttggagactctggagaggagataaataaatg-3′ (positive control).

Immunofluorescence Staining

Translocation of NF-κB (p65) was analyzed by immunofluorescence staining as described previously [38]. Primary cortical neurons were fixed in 4 % paraformaldehyde for 15 min at RT and then permeabilized with 0.1 % Triton X-100 for 10 min and incubated with blocking buffer (10 % BSA in PBS) for 1 h at RT. Primary neurons were incubated with rabbit anti-p65 (1:500) or goat anti-p22phox (1:250; both from Santa Cruz Biotechnology) overnight at 4 °C and then with Cy3-conjugated goat anti-rabbit or Cy2-conjugated donkey anti-goat (1:1000; Jackson ImmunoResearch, West Grove, PA, USA) for 2 h at RT. Primary neurons were stained with Hoechst 33342 for nuclei (5 μg/ml in PBS, 10 min at RT; Sigma Chemical Co, St. Louis, MO, USA) and then wet mounted and observed by confocal microscopy (LSM710, Carl Zeiss, Jena, Germany).

Stroke Model

The focal cerebral ischemia model entailing three-vessel occlusion was as reported [47]. In brief, 8- to 10-week-old male Long-Evans rats purchased from *The National Laboratory Animal Center* (NLAC; Taipei, Taiwan) were anesthetized with chloral hydrate (360 mg/kg body wt, IP), with the right middle cerebral artery (MCA) ligated reversibly with a 10-0
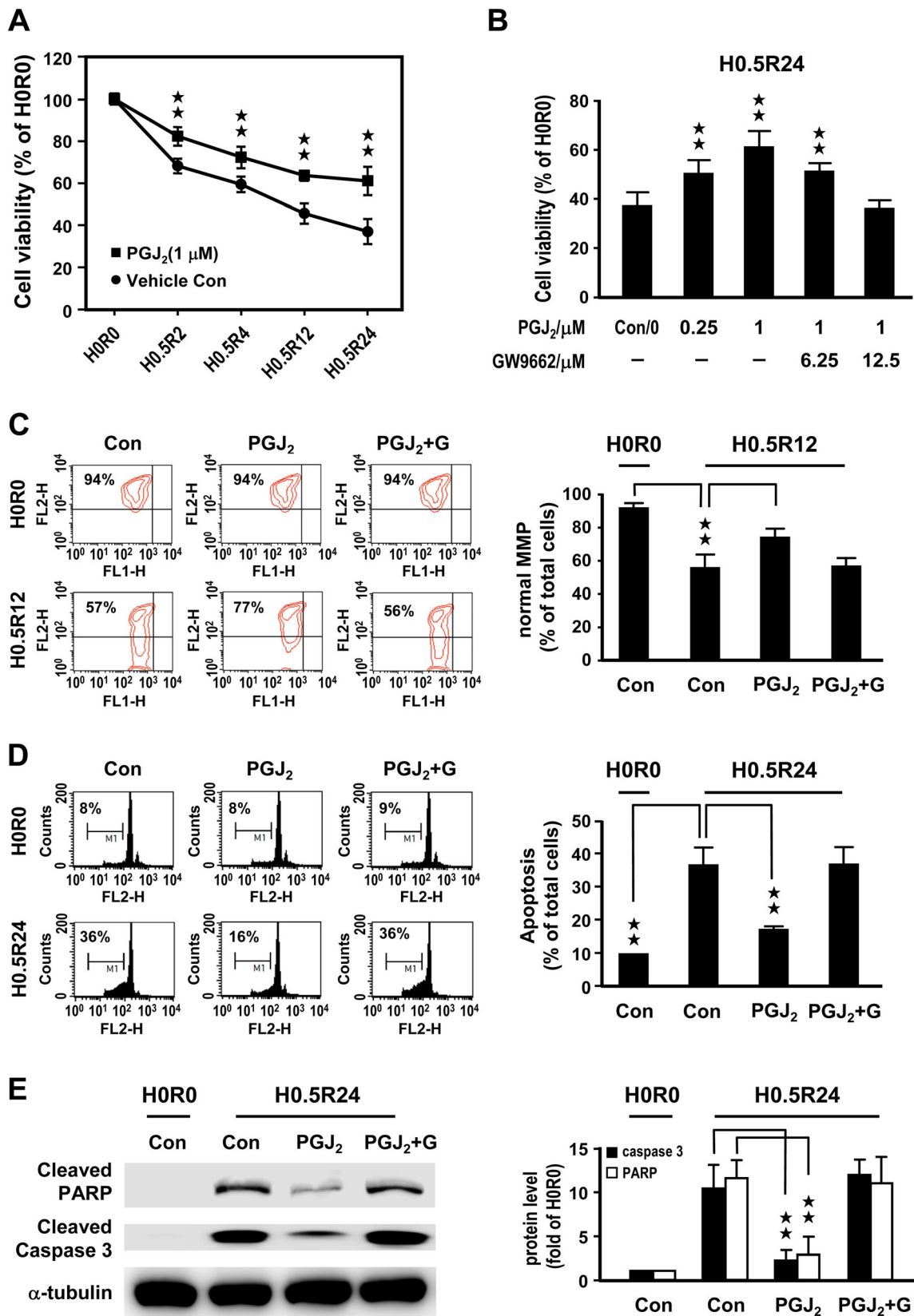
Fig. 1 15d-PGJ$_2$ protects primary cortical neurons (PNs) from OGD-induced death in a PPAR-γ-dependent manner. PNs pretreated with 15d-PGJ$_2$ for 12 h underwent OGD for 0.5 h then reoxygenation for 2 to 24 h (H0.5R2~H0.5R24) for cell viability analysis (**a**). PNs pretreated with 15d-PGJ$_2$ or in various combinations with GW9662 (or G) were analyzed for cell viability at H0.5R24 (**b**), normal mitochondrial membrane potential (MMP) at H0.5R12 (**c**), or apoptosis at H0.5R24 (**d**) and cleaved caspase-3 and PARP-1 levels at H0.5R24 (**e**). H0R0 refers to no OGD vehicle control. Data are mean ± SD of at least three independent experiments performed in triplicate. $^{\star\star}P<0.01$ versus control
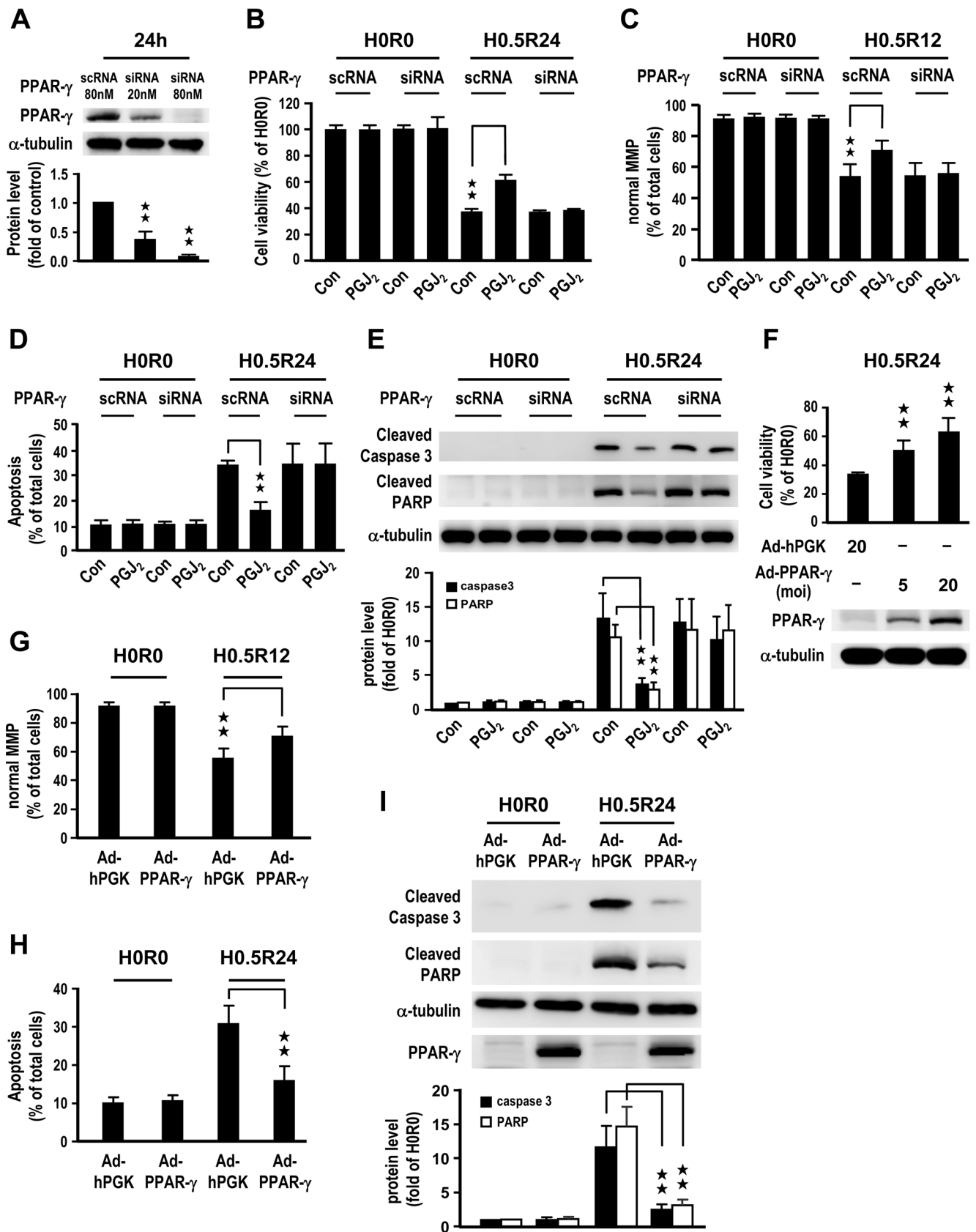
Fig. 2 Protective effect of 15d-PGJ$_2$ was abolished by PPAR-γ siRNA knockdown while mimicked by Ad-PPAR-γ overexpression. The transfection efficacy of PPAR-γ siRNA to primary cortical neurons (PNs) was analyzed after 24-h transfection (**a**). PNs were transfected with 80 nM PPAR-γ siRNA, treated with 1 μM 15d-PGJ$_2$ and then underwent H0.5R12 or H0.5R24 for analysis of cell viability (**b**), normal MMP (**c**), apoptosis (**d**), or cleaved caspase-3 and PARP-1 protein levels (**e**). The infection efficacy of 24-h Ad-PPAR-γ and its effect on PNs viability (**f**), normal MMP (**g**), apoptosis (**h**), and cleaved caspase-3 and PARP-1 protein levels (**i**) were analyzed at H0.5R12 or H0.5R24. H0R0 refers to no OGD normal control. Data are mean ± SD of at least three independent experiments performed in triplicate. ★★$P<0.01$ versus control

suture and both common carotid arteries (CCAs) occluded also reversibly with aneurysm clips. Triple vessel occlusion was held for 35 min and then the suture and the aneurysm clips were released with restoration of blood flow in the three arteries verified. Animals were kept in an air-ventilated incubator at 24.0±0.5 °C and sacrificed under anesthesia at variable intervals after focal cerebral ischemia. Brains were removed and the ischemic and contralateral cerebral cortices isolated and frozen. Infarct area was delineated by 2,3,5-triphenyltetrazolium chloride (TTC) and infarct volume measured as previously described [47]. All procedures were performed in accordance with the Public Health Service Guide Approved Procedures for the Care and Use of Laboratory Animals and approved by the Academia Sinica Animal Studies Committee (IACUC, http://iacuc.sinica.edu.tw/). All siRNA treatments were performed in random order, by an investigator blinded to the surgical groups.

Intracerebral Ventricular (icv) Infusion of p22phox siRNA

The procedure was performed as previously described [34, 46]. Briefly, anesthetized rats were placed in a stereotaxic apparatus; 10 μl of artificial cerebrospinal fluid containing 0.125~0.5 ng of p22phox siRNA was infused into the right lateral ventricle at a rate of 2 μl/min at the following coordinates: anterior, 2.5 mm caudal to bregma; right, 2.8 mm lateral to midline; and ventral, 3.0 mm ventral to dural surface. Rats were infused with siRNA right after 30 min MCA occlusion. Periodic confirmation of proper placement of the needle was performed with infusion of fast green.

RNA Isolation, Reverse Transcription, and Polymerase Chain Reaction

RNA isolation was performed as previously described [34]. Total RNA (4 μg) was incubated with RevertAid™ H Minus First Strand cDNA Synthesis Kit (Fermentas, Vilnius, Lithuania). The reaction mixture was incubated at 65 °C for polydT oligomer annealing and then extension in buffer, dNTP, reverse transcriptase, and RNase inhibitor in a final

volume of 20 μl at 42 °C for 1 h and then 70 °C for 5 min to inactivate the enzyme. Finally, a total of 80 μl DEPC-treated water was added to the reaction mixture before storage at −80 °C. One to 2 μl of the RT reaction solution was used in the PCR reaction. PCR was carried out in a 25-μl final volume containing 0.2 mM dNTP, 0.1 μM of each primer, and 1 unit of Taq polymerase (NEB, Ipswich, MA). The mixture was subjected to PCR amplification for 25~30 cycles, incubated at 72 °C for 10 min, and then cooled to 4 °C (PE, Norwalk, CT). The primers were as follows: for rat-p22 F: 5′-ctctattgttgcag gagtgc-3′, R: 5′-tcacacgacctcatctgtcac-3′; mouse-p22 F: 5′-tggcctgattctcatcactg-3′, R: 5′-taggtggttgcttgatggtg-3′; and rat/mouse-β-actin F: 5′-catccgtaaagacctctatgccaac-3′, R: 5′-caaagaaagggtgtaaaacgcagc-3′.

Protein Oxidation Detection

To assess the formation of protein carbonyl groups, the OxyBlot protein oxidation detection kit (Millipore, Billerica, MA) was used according to the manufacturer's protocol. In brief, protein samples were prepared from rat brains harvested at 24 h after MCAO. Subsequently, 10 μl protein sample (30 μg) was added with 10 μl of 12 % SDS and 20 μl of 1× 2,4-dinitrophenylhydrazine (DNPH) solution into a tube. Twenty microliters of 1× neutralization solution instead of the DNPH solution served as the negative control. Tubes were incubated at room temperature for 15 min. Neutralization solution (20 μl) was added to each tube, and one mixed sample per lane was loaded onto 10 % Tris-glycine gels. Following electrophoresis and transfer to PVDF membranes, which were blocked in Tris buffer containing 0.1 % Tween 20 for 1 h at RT, membranes were incubated 1.5 h at RT with the primary antibody stock (1:5000) and then incubated with secondary antibodies (1:20,000) at RT for 1 h. Blots were developed by an enhanced chemiluminescence detection system (Millipore, Billerica, MA). Proteins that underwent oxidative modification (i.e., carbonyl group formation) were identified. Levels of oxidatively modified proteins were quantified by the MetaMorph image analysis software.

Behavioral Assessment

Rats after MCAO exhibited unilateral forelimb weakness and flexion with reduced resistance when suspended by tail and applied pressure on their shoulders. *Bederson's test* was used to evaluate neurological deficits based on these postural reflexes before MCAO and 7 days after MCAO by investigators blinded to the study conditions. Rats were scored based on the following criteria: grade 5 (normal); grade 4 (forelimb flexion and no other abnormalities); grade 3 (reduced resistance to lateral push toward the paretic side and forelimb flexion); grade 2 (same behavior as grade 3, with circling toward the
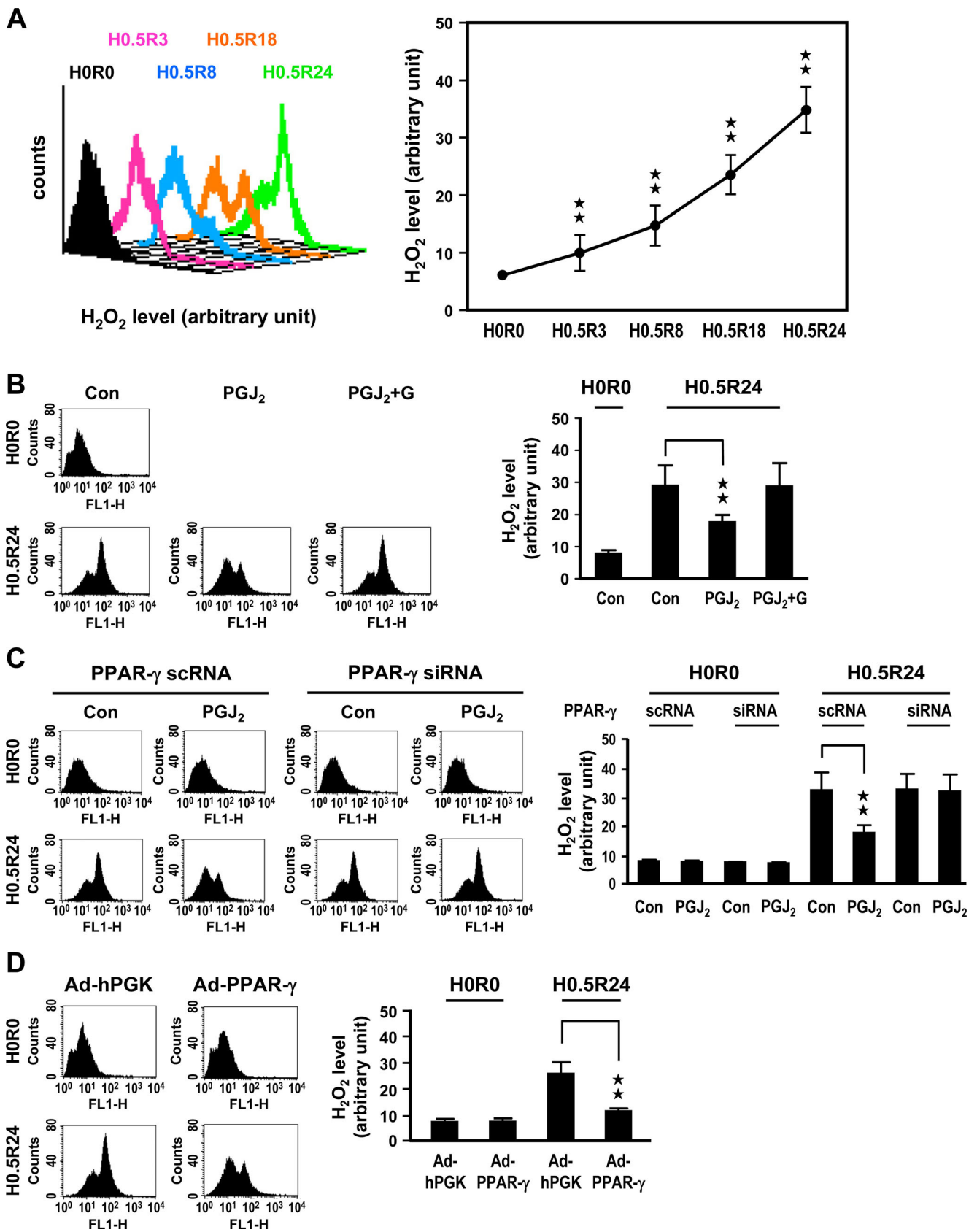
◀ **Fig. 3** 15d-PGJ$_2$ attenuates OGD-induced ROS/H$_2$O$_2$ accumulation in a PPAR-γ-dependent manner. PNs were subjected to 0.5-h OGD and reoxygenation for 3 to 24 h (H0.5R3 to H0.5R24). The temporal histograms of ROS levels were derived from DCFH oxidation and quantified by flow cytometry (**a**). PNs without (**b**) or with (**c**) 80 nM PPAR-γ siRNA transfection were pretreated with 1 μM 15d-PGJ$_2$ or in combination with 12.5 μM GW9662 (or G), then underwent H0.5R24 for ROS determination. PNs infected with 20 moi Ad-PPAR-γ underwent H0.5R24 for ROS determination (**d**). H0R0 refers to no OGD normal control. Data are mean ± SD of at least three independent experiments performed in triplicate. ★★$P<0.01$ versus control

paretic side when pulling the tail on the table); grade 1 (same behavior as grade 2, with spontaneous circling); and grade 0, no activity [48]. Using the *elevated body swing test*, animals were examined for asymmetrical motor behavior. Animals were held by the tail and elevated about an inch from the bottom of a Plexiglas box. During the 20-s trial, the direction and number of times that the animal moved more than 10° to either the left or right side of the vertical axis were recorded. Each animal had to return to the vertical position before the next swing was counted. Intact animals do not exhibit a uniform side-biased swing although individual animals may exhibit a preferential side-biased swing [49]. All the experiments were run by a trained investigator blinded to the experimental conditions.

Magnetic Resonance Imaging Experiment

Magnetic resonance imaging (MRI) studies were performed on a 7-T PharmaScan 70/16 MR scanner (Bruker Biospin GmbH, Germany) with an active shielding gradient (30 G/cm in 80 μs). Rats were initially anesthetized with 5 % isoflurane and maintained with 1.5 to 2.0 % isoflurane at 2 l/min air flow. Rats were allowed to breathe spontaneously throughout the experiments. Rats were placed in a prone position and fitted with a custom-designed head holder inside the magnet, as previously described [50]. Images were acquired using a 72-mm birdcage transmitter coil and a separate quadratic surface coil for signal detection. Multislice axial FES T2WI was acquired with a field of view of 3.0×3.0 cm^2, a matrix size of 256×128 with zero-filling to 256×256, repetition time=4500 ms, echo time=70 ms, bandwidth=50 kHz, slice thickness=1 mm, number of averages=8, and the total acquisition time is 9 min 36 s. T2WI was assessed by TMC core service engineers blinded to the study conditions at 14 days after ischemia.

Statistical Analysis

ANOVA was used to compare the expression of proteins, mRNA, or infarct volumes. Differences between groups were further analyzed by post hoc Fisher's protected t test by the use of GB-STAT 5.0.4 (Dynamic Microsystems, Silver

Springs, MD). $P<0.05$ was considered significant. We use at least $n=3$ in triplicates for in vitro studies and $n\geq6$ for in vivo studies.

Results

15d-PGJ$_2$ Protects Mouse Primary Cortical Neurons Against OGD-Induced Death via a PPAR-γ-Dependent Pathway

To study the protective mechanism of 15d-PGJ$_2$, primary cortical neurons (PNs) were subjected to 0.5-h OGD and then reoxygenation for 2 to 24 h. Cell viability slowly decreased with progressive reoxygenation (Fig. 1a). About 68 % of cells survived after 2-h reoxygenation (H0.5R2), and only 38 % of cells remained viable at 24-h reoxygenation (H0.5R24). PN pretreatment with 1 μM 15d-PGJ$_2$ for 12 h showed a significant increase in cell viability at 2 to 24 h of reoxygenation (Fig. 1a). 15d-PGJ$_2$ concentration-dependently attenuated PN death after 0.5-h OGD and 24-h reoxygenation (H0.5R24) insult (Fig. 1b). This protective effect was abrogated by GW9662, a PPAR-γ antagonist (Fig. 1b); 24-h pretreatment with GW9662 per se did not alter cell viability.

To study the cell death signaling that 15d-PGJ$_2$ interrupted, we examined the population of normal MMP and sub-G$_0$/G$_1$ (i.e., apoptosis) in PNs by flow cytometry using JC-1 and PI staining. PNs subjected to H0.5R12 showed reduced normal MMP population (55.4±8 %); pretreatment with 1 μM 15d-PGJ$_2$ significantly upheld the normal MMP cell population (73±6.3 %); this protective effect was abrogated by 12.5 μM GW9662 (Fig. 1c). In addition, H0.5R24 treatment increased apoptotic population (36.5±4.8 %), and pretreatment with 15d-PGJ$_2$ significantly lessened apoptotic population (16.9±1.1 %); this preventive effect was neutralized by GW9662 (Fig. 1d). To ascertain whether the beneficial effect of 15d-PGJ$_2$ was via mitochondria-dependent apoptosis, we analyzed the proapoptotic markers, cleaved caspase-3 and PARP-1. Cleaved caspase-3 and PARP-1 protein levels were greatly enhanced after H0.5R24 challenge while relieved by 15d-PGJ$_2$, which was counteracted by GW9662 (Fig. 1e).

PPAR-γ siRNA knockdown and gene transfer were used to confirm that 15d-PGJ$_2$ prevents PNs from OGD-induced MMP breakdown and apoptosis via PPAR-γ. Transfection of PPAR-γ siRNA for 24 h concentration-dependently decreased PPAR-γ protein level as compared to the scRNA control (Fig. 2a). In PNs transfected with PPAR-γ siRNA, 15d-PGJ$_2$ was unable to attenuate OGD-induced cell death (Fig. 2b), MMP breakdown (Fig. 2c), apoptosis (Fig. 2d), and caspase-3 activation (Fig. 2e). Meanwhile, PPAR-γ over-expression, by adenovirus-PPAR-γ (Ad-PPAR-γ) infection for 24 h, concentration-dependently increased PPAR-γ levels as compared with the Ad-hPGK control in PNs (Fig. 2f; lower
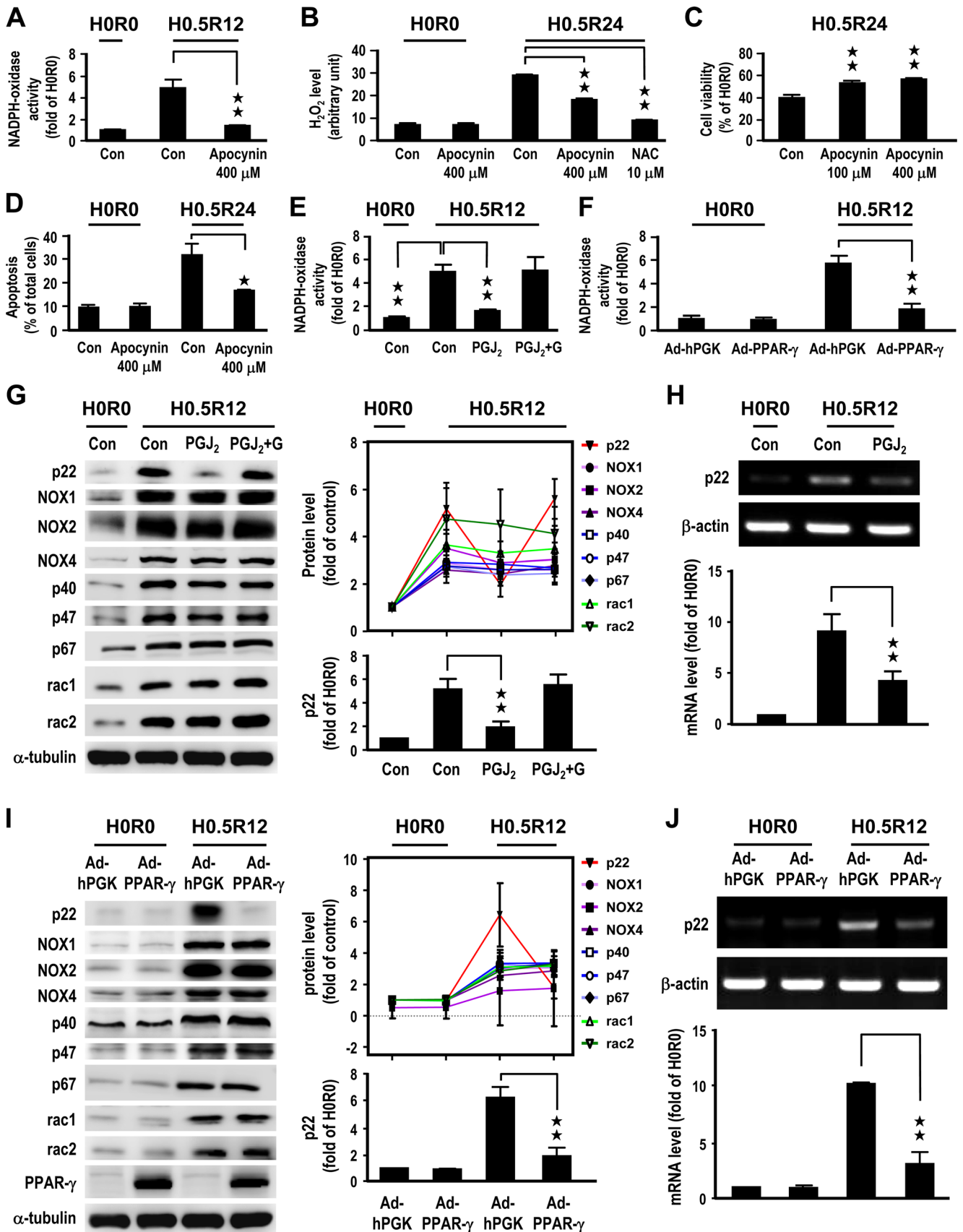
◀ **Fig. 4** 15d-PGJ$_2$ inhibits OGD-induced NADPH oxidase activation and p22phox expression in a PPAR-γ-dependent manner. PNs were pretreated with apocynin or NAC and underwent H0.5R12 or H0.5R24 for NADPH oxidase activity (**a**), ROS levels (**b**), cell viability (**c**), and apoptosis (**d**) analysis. PNs were pretreated with 1 μM 15d-PGJ$_2$ or in combination with 12.5 μM GW9662 (**e**), or were infected with 20 moi Ad-PPAR-γ (**f**), then subjected to H0.5R12 for NADPH oxidase activity determination. PNs were pretreated with 1 μM 15d-PGJ$_2$ or in combination with 12.5 μM GW9662 (**g**, **h**), or were infected with 20 moi Ad-PPAR-γ (**i**, **j**), then subjected to H0.5R12 for NADPH oxidase subunits protein level analysis (**g**, **i**), or p22phox mRNA determination (**h**, **j**). H0R0 refers to no OGD normal control. Data are mean ± SD of at least three independent experiments performed in triplicate. ★★$P<0.01$ versus control

panel). PPAR-γ overexpression, mimicking 15d-PGJ$_2$, could ameliorate OGD-induced cell death (Fig. 2f; upper panel), MMP breakdown (Fig. 2g), apoptosis (Fig. 2h), and caspase-3 activation (Fig. 2i). Hence, PPAR-γ is a neuroprotectant and 15d-PGJ$_2$-PPAR-γ signaling protects PNs against OGD insult.

15d-PGJ$_2$-PPAR-γ Attenuates OGD-Induced Apoptotic Neuronal Death via Inhibiting NADPH Oxidase and Subsequent ROS Generation in PNs

Excessive ROS induces apoptosis through both extrinsic and intrinsic pathways in the ischemic brain. ROS sensing dye DCFH-DA was used to examine the role of ROS in OGD-induced apoptosis in PNs. OGD reoxygenation resulted in a gradual increase in ROS level up to 24 h of reoxygenation (H0.5R3~H0.5R24) (Fig. 3a). Most of the ROS were noted in the reoxygenation phase, and this ROS accumulation was mitigated by 15d-PGJ$_2$. The ROS-lowering effect of 15d-PGJ$_2$ was counteracted by PPAR-γ antagonist GW9662 or siRNA while mimicked by Ad-PPAR-γ at H0.5R24 (Fig. 3b–d).

We then investigated whether 15d-PGJ$_2$-PPAR-γ attenuated ROS level by inhibiting NADPH oxidase activity, since NOX is a major source of ROS generation in reoxygenation/ reperfusion phase after ischemia. NOX was activated in PNs subjected to H0.5R12 and can be repressed by NOX inhibitor apocynin (Fig. 4a). Apocynin or N-acetylcysteine (NAC) pretreatment mitigated ROS formation (Fig. 4b), cell death (Fig. 4c), and apoptosis (Fig. 4d) in PNs subjected to H0.5R24. Concurrently, OGD-induced NOX activation was also inhibited by 15d-PGJ$_2$ (Fig. 4e). The ability of 15d-PGJ$_2$ to inhibit NADPH oxidase was offset by GW9662, a PPAR-γ antagonist (Fig. 4e), while mimicked by Ad-PPAR-γ (Fig. 4f). These results support that 15d-PGJ$_2$-PPAR-γ, via inhibiting NOX, downregulates OGD-induced ROS and subsequent PNs apoptosis.

To dissect the underlying inhibitory mechanism of 15d-PGJ$_2$-PPAR-γ, we examined the protein level of individual subunits of NOX after OGD insult. A significant increase in the level of all examined subunits was noted following H0.5R12 challenge in PNs (Fig. 4g); surprisingly, p22phox,

both protein and mRNA, was the only subunit repressed by 15d-PGJ$_2$ (Fig. 4g, h). The ability of 15d-PGJ$_2$ to inhibit OGD-induced p22phox expression was neutralized by GW9662, a PPAR-γ antagonist (Fig. 4g), while mimicked by Ad-PPAR-γ (Fig. 4i, j). These findings together suggest that 15d-PGJ$_2$-PPAR-γ inhibited OGD-induced NADPH oxidase activation via decreasing p22phox subunit level.

15d-PGJ$_2$-PPAR-γ via Inhibiting NF-κB Nuclear Translocation Downregulates OGD-Induced p22phox Transcription

Since both p22phox mRNA and protein were downregulated, PPAR-γ, as a transcription factor, might regulate p22phox at the transcriptional level. We analyzed the mouse p22phox promoter region by the MAPPER search engine and deduced one potential PPAR-γ binding site and one potential NF-κB binding site (Fig. 5). We then cloned four 5′-flanking regions of p22phox gene into pGL4 luciferase reporter vectors: (1) p1323-Luc: a 1323-bp (−1323 to 1) 5′-flanking region of the mouse genome that harbors both PPAR-γ (−1167 to −1155) and NF-κB (−347 to −338) binding sites; (2) p482-Luc: a PPAR-γ binding site truncated p1323-Luc (−482 to 1); (3) p100-Luc: both PPAR-γ and NF-κB binding sites truncated p1323-Luc (−100 to 1); and (4) Dp1323-Luc: a NF-κB binding site deleted p1323-Luc, sequence −354 to −332 were deleted (Fig. 5). To determine the role of PPAR-γ in p22phox transcription, N2A cells were transfected with various p22phox reporter constructs 24 h before subjected to H0.5R12. N2A cells were used for this set of experiments because of the technical difficulty in transfection studies with primary cortical neurons. The p1323-Luc reporter was turned on following H0.5R12 challenge, and 15d-PGJ$_2$ concentration-dependently decreased p1323-Luc reporter activity (Fig. 5a). This reporter inhibitory effect of 15d-PGJ$_2$ was counteracted by GW9662 and PPAR-γ siRNA while mimicked by Ad-PPAR-γ (Fig. 5a–c). Surprisingly, p482-Luc reporter was also turned on following H0.5R12 challenge, and pretreatment with 15d-PGJ$_2$ also decreased p482-Luc reporter activity, despite that the PPAR-γ binding site was deleted (Fig. 5d). Furthermore, H0.5R12 challenge did not turn on the p100-Luc reporter, with both PPAR-γ and NF-κB binding sites deleted (Fig. 5d), indicating the involvement of NF-κB in p22phox transcription. The importance of the NF-κB binding site was further confirmed by the observation that (1) H0.5R12 challenge did not turn on the Dp1350-Luc reporter, with the NF-κB binding site deleted, despite the presence of the PPAR-γ binding site; (2) cotransfection with constitutively activated N-terminal truncated IκBα mutant plasmid (△N-I-κBα, a generous gift from Dr. Chou-Zen Giam), which retains NF-κB in the cytoplasm and blocks NF-κB activation, decreased p1323-

Mouse p22phox reporter construct
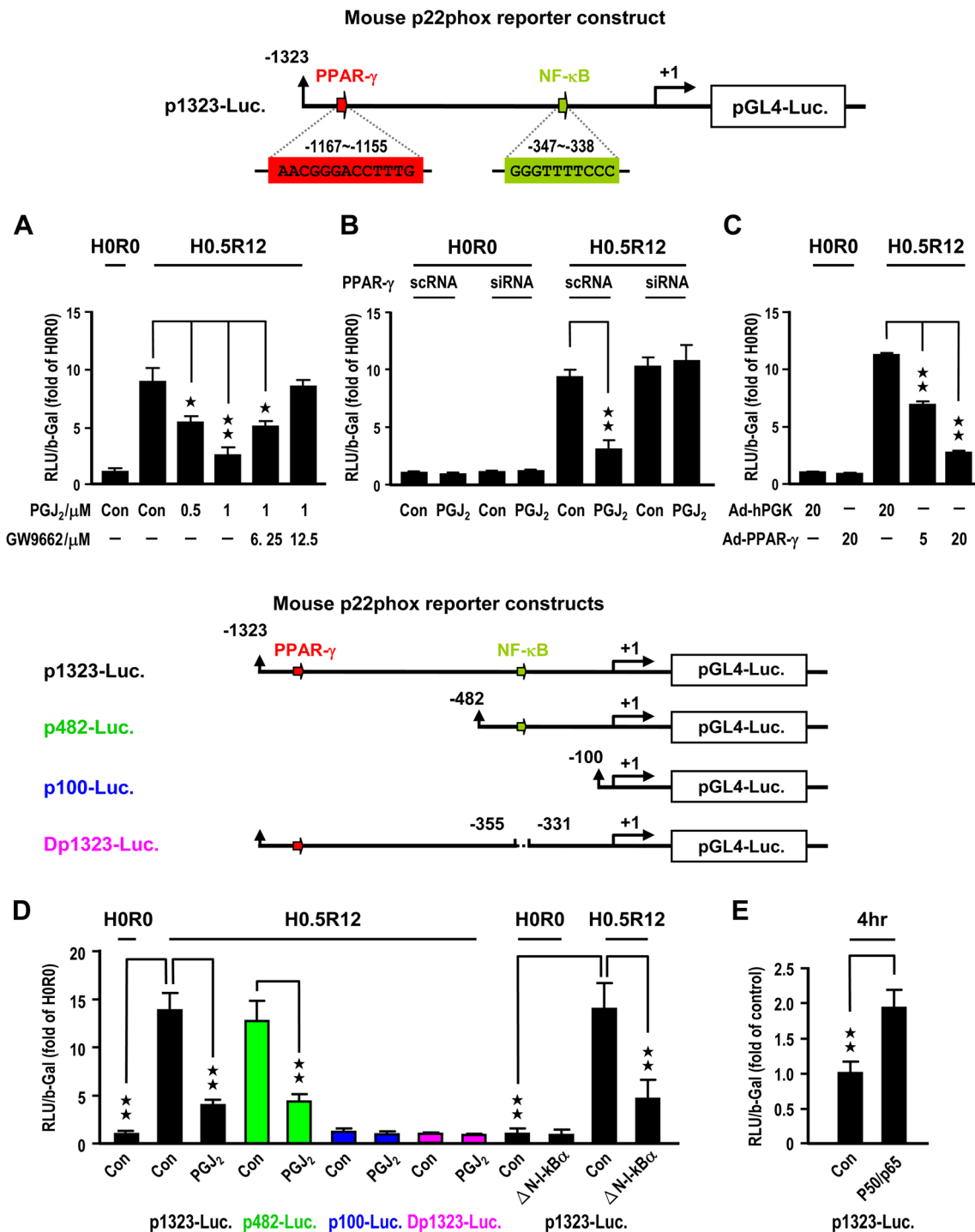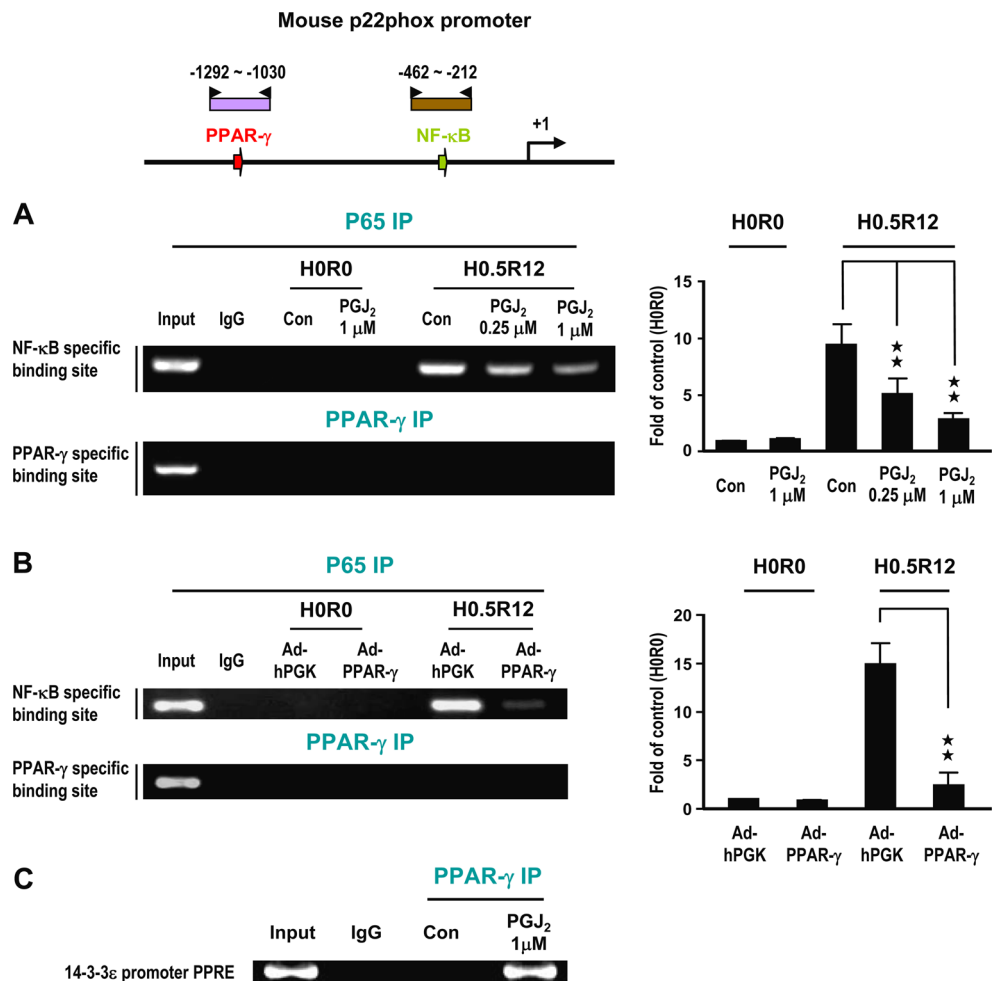

Mouse p22phox reporter constructs

Fig. 5 15d-PGJ$_2$-PPAR-γ suppresses NF-κB-driven p22phox transcription after OGD insult. Human neuroblastoma N2A cells were transfected with 0.5 μg p1323-Luc before (**a**) pretreatment with 15d-PGJ$_2$ or in combination with GW9662; (**b**) transfected with 80 nM PPAR-γ siRNA and treatment with 1 μM 15d-PGJ$_2$; or (**c**) infected with 20 moi Ad-PPAR-γ, then subjected to H0.5R12 for p22phox reporter assay. N2A cells were either transfected with 0.5 μg p1323-Luc, p482-Luc, p100-Luc, or Dp1323-Luc

before treatment with 1 μM 15d-PGJ$_2$; or cotransfected with p1323-Luc and △N-I-κBα, then subjected to H0.5R12 for p22phox reporter assay (**d**). N2A cells were cotransfected with 0.5 μg p1323-Luc and P50/p65 plasmids 4 h for reporter assay (**e**). Reporter activity is expressed as relative light units (RLU) with β-gal (b-Gal) as a normalization control. H0R0 refers to no OGD normal control. Data are mean ± SD of at least three independent experiments performed in triplicate. ★$P<0.05$ and ★★$P<0.01$ versus control

Luc reporter activity (Fig. 5d); as well as (3) cotransfection with NF-κB (p50/p65) plasmids for 4 h increased p1323-Luc reporter activity (Fig. 5e).

ChIP analysis further confirmed the binding of NF-κB, not PPAR-γ, onto p22phox promoter, and 15d-PGJ$_2$ concentration-dependently decreased NF-κB binding to

the p22phox promoter in PNs subjected to H0.5R12 challenge (Fig. 6a). Concurrently, PPAR-γ overexpression by Ad-PPAR-γ attenuated NF-κB binding to the p22phox promoter, yet left the PPAR-γ binding site idle (Fig. 6b). Binding of PPAR-γ to 14-3-3ε promoter serves as a technical control (Fig. 6c). Thus, 15d-PGJ$_2$-PPAR-γ signaling, via lowering NF-κB binding onto p22phox promoter, downregulated its transcription.

The subcellular NF-κB levels were further analyzed. Despite the total level of p65 protein, one of the key subunits of NF-κB was not altered in whole cell lysates of PNs subjected to H0.5R12, and p65 level was decreased in the cytosol while increased in the nucleus after OGD insult (Fig. 7a, b). Pretreatment with 15d-PGJ$_2$ did not alter the total p65 level but restrained the translocation of NF-κB from the cytosol to the nucleus (Fig. 7a, b). The translocation inhibitory effect of 15d-PGJ$_2$ was counteracted by GW9662, a PPAR-γ antagonist, while mimicked by Ad-PPAR-γ (Fig. 7b, c). Immunocytochemical studies further revealed that following H0.5R12 challenge, NF-κB (p65) migrated from the cytosol into the nucleus in PNs, while pretreatment with 15d-PGJ$_2$ blocked this translocation (Fig. 7d; upper). The downstream p22phox

protein was increased after H0.5R12 challenge, while pretreatment with 15d-PGJ$_2$ suppressed the expression of p22phox (Fig. 7d; lower). These observations support the pivotal role of NF-κB in p22phox transcription.

Postischemic p22phox siRNA Treatment Ameliorates Protein Oxidation, Neuronal Death, Cerebral Infarct, and Neurological Deficit

To determine the impact of p22phox downregulation on hypoxic neuronal death, PNs were transfected with p22phox siRNA for 24 h and then subjected to H0.5R24. Cell survival was increased (Fig. 8a), while H$_2$O$_2$ levels and NOX activity were decreased (Fig. 8b, c) in PNs transfected with p22phox siRNA as compared with scRNA controls. p22phox siRNA concentration-dependently decreased p22phox protein level in PNs (Fig. 8a; lower panel). To investigate whether the in vitro findings could be translated into ischemic brain in vivo, we further assessed the effect of postischemic p22phox siRNA treatment, immediately after 30-min MCA occlusion or at the onset of reperfusion, on ischemic brain injury. At 24-h (1D) reperfusion, infarct volumes were
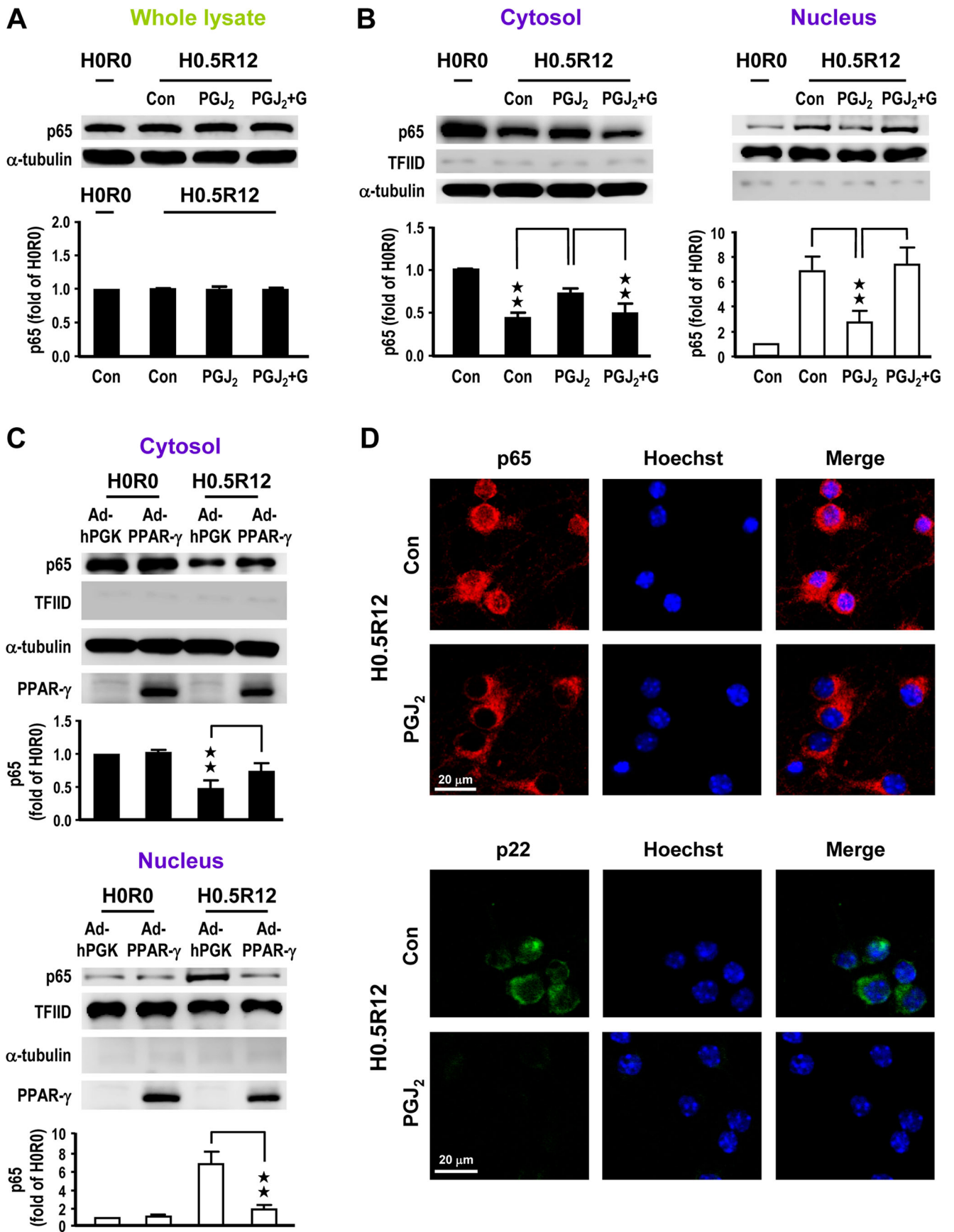
◀ **Fig. 7** 15d-PGJ$_2$ and PPAR-γ inhibit the translocation of cytosolic NF-κB (p65) to nucleus. PNs were (**a**), (**b**) pretreated with 1 μM 15d-PGJ$_2$ or in combination with 12.5 μM GW9662, or (**c**) infected with 20 moi Ad-PPAR-γ, then subjected to H0.5R12 for subcellular localization of NF-κB (p65). TFIID and α-tubulin were included as a loading control for nuclear and cytosolic fractions, respectively. H0R0 refers to no OGD normal control. Data are mean ± SD of at least three independent experiments performed in triplicate. ★★$P<0.01$ versus control. (**d**) A representative immunofluorescence staining of subcellular localization of NF-κB (p65; *red*) and p22phox (*green*) in PNs of **b**. Hoechst 33342 (*blue*) was included as nuclear marker. Similar results were observed in two other sets of experiments

reduced by p22phox siRNA in a dose-dependent manner (Fig. 8d). Levels of p22phox mRNA (Fig. 8e) and protein oxidation (Fig. 8f) were significantly decreased in the ischemic cortices of rats transfected with p22phox siRNA relative to scRNA controls. Meanwhile, cleaved PARP-1, cleaved caspase-3, and p22phox levels were lowered in the p22phox siRNA-treated group than scRNA controls, yet leaving p-IκBα levels unaltered, an index of NF-κB activation (Fig. 8g), suggesting that NF-κB is upstream of p22phox. In addition, at 7 days (1 W) after ischemia, sustained smaller infarct volumes were noted in the p22phox siRNA-treated group by T2-weighted images (Fig. 9a). Lastly, postischemic p22phox siRNA treatment also resulted in better functional outcome based on Bederson's postural reflex task (Fig. 9b) and elevated body swing test (Fig. 9c).

Discussion

It is well established that NOX is a major mechanism for ROS generation following brain ischemia, especially in the reoxygenation/reperfusion phase [4, 13, 51]. PPAR-γ agonism lowered oxidative stress to ameliorate ischemic neuronal death via enhancing the expression of ROS scavenging genes [32, 52, 53]. Whether PPAR-γ also acts on NOX, a ROS generating gene to reduce oxidative stress and ischemic neuronal death has not been previously reported. In the present study, we demonstrated that PPAR-γ, via attenuating NF-κB nuclear translocation, suppressed subsequent p22phox transcription, NOX activation, neuronal apoptosis, and brain damage.

Previously, we have shown that 15d-PGJ$_2$ and rosiglitazone suppressed brain infarction and neuronal apoptosis in a PPAR-γ-dependent manner [34, 42]. OGD-induced ROS/H$_2$O$_2$ accumulation and neuronal apoptosis were attenuated by rosiglitazone via PPAR-γ [43]. Here we shown that majority of the OGD-induced ROS was accumulated during reoxygenation/reperfusion, suggesting the involvement of NOX [51]. With pharmacological (PPAR-γ antagonist GW9662), loss-of-function (PPAR-γ siRNA), and gain-of-function (Ad-PPAR-γ) approaches, we further elaborated that (1) 15d-

PGJ$_2$-PPAR-γ signaling inhibited NOX-dependent ROS generation, which contributed to neuronal apoptosis after OGD insult; and (2) this antioxidative activity of 15d-PGJ$_2$-PPAR-γ is accompanied by a selective downregulation of p22phox expression, the regulatory subunit of NOX which is responsible for anchoring and integrating of Noxs and cofactors to the plasma membrane. These observations support a causal and specific link of PPAR-γ to NOX in this neuroprotective paradigm.

Since both p22phox protein and mRNA levels were decreasing, consistent with the role of PPAR-γ as a transcription factor, we deduced one PPAR-γ binding site (PPRE) and one NF-κB binding site (κBRE) in the promoter region of p22phox gene by the MAPPER search engine. Reporter assays revealed that NF-κB is critical for OGD-induced p22phox transcription, which was suppressed by 15d-PGJ$_2$-PPAR-γ. Results of ChIP assay further confirmed that OGD insult led to the binding of NF-κB to κBRE, but not PPAR-γ to PPRE, on p22phox promoter and triggering its transcription. Neither 15d-PGJ$_2$ nor Ad-PPAR-γ pretreatment induced the binding of PPAR-γ to PPRE; however, a concurrent decrease in NF-κB binding to κBRE on p22phox promoter was observed. Of note, under the same experimental conditions, we did observe the binding of PPAR-γ to PPRE on 14-3-3ε promoter reported by our group [34]. These findings testify the multilevel and multidimensional capability of PPAR-γ in modulating a variety of genes to protect ischemic neurons. However, the mechanisms underlying the differential gene regulation remain to be established. Subcellular localization studies further uncovered that, despite the total level of NF-κB not being altered, OGD-induced NF-κB nuclear translocation was attenuated by 15d-PGJ$_2$ or Ad-PPAR-γ in hypoxic neurons. Collectively, 15d-PGJ$_2$-PPAR-γ via attenuating NF-κB nuclear translocation lessened NF-κB-driven p22phox transcription. Although pioglitazone, a synthetic PPAR-γ agonist, has also been shown to inhibit NF-κB nuclear translocation in a permanent MCA occlusion model, its causal relationship with ROS-related genes was not studied [54]. NF-κB functions as a hub to regulate a myriad of biological processes. NF-κB activation/translocation is regulated by sequential phosphorylation and ubiquitination of TAK1, IKK complex, and IκBα [55]. Further studies are needed to address the mechanisms underlying the inhibition of NF-κB translocation by PPAR-γ (Fig. 10).

Noteworthily, p22phox siRNA knockdown is associated with decreasing NOX activity and ROS generation while increasing cell survival in hypoxic neurons. The pivotal role of p22phox in ischemic brain injury is further supported by the original findings that postischemic p22phox knockdown by p22phox siRNA not only reduced infarct volumes but also improved functional outcome at 1 week after transient ischemic insult. The neuroprotective action of p22phox siRNA was accompanied by a decrease in the levels of p22phox and
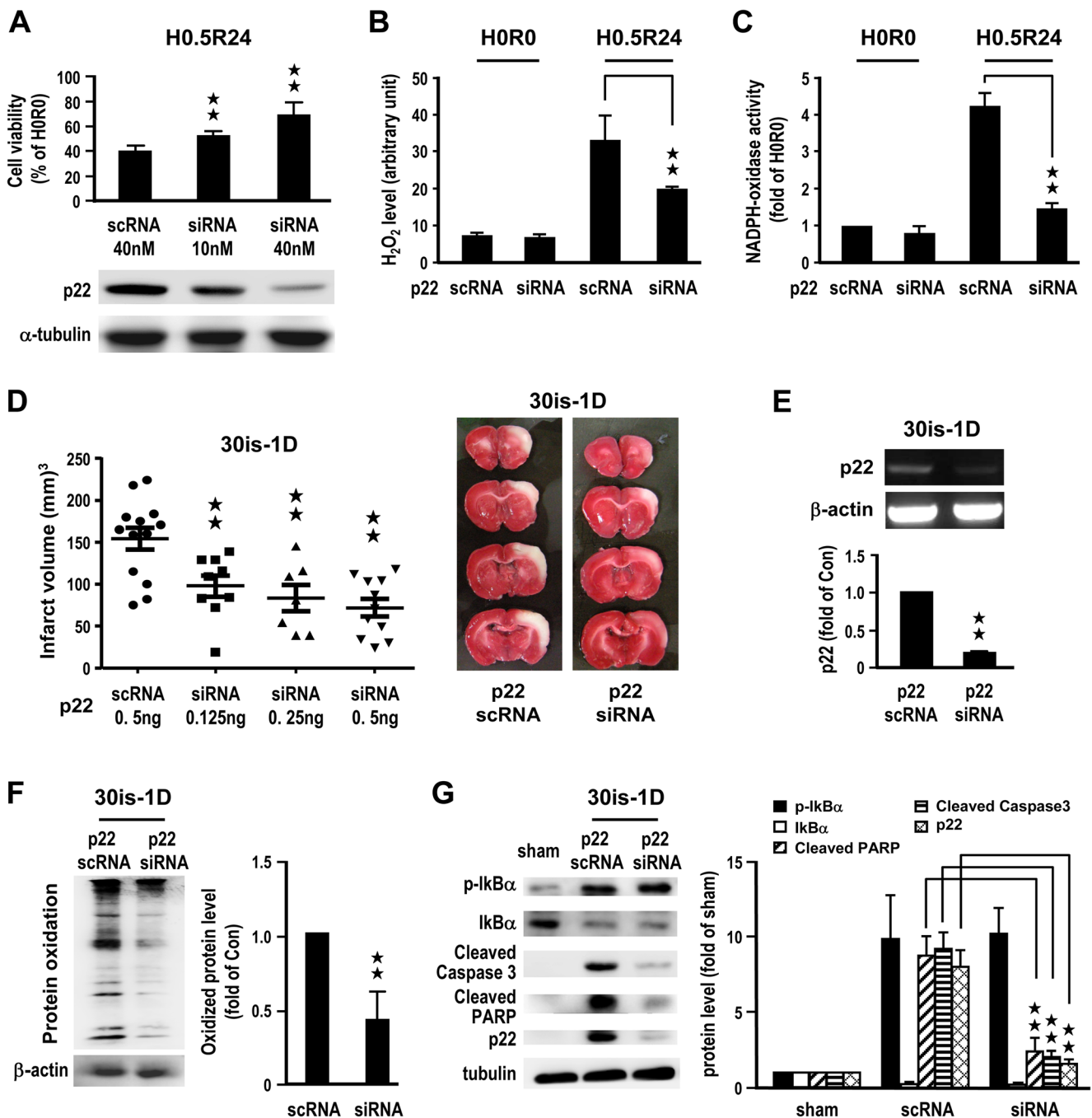
Fig. 8 P22phox siRNA treatment reduces PNs death and brain infarct. PNs transfected with 40 nM p22phox siRNA were subjected to H0.5R12 or H0.5R24 for cell viability (**a**), ROS level (**b**), and NOX activity (**c**) analyses. The efficacy of p22phox siRNA was evaluated by western blot in PNs at H0.5R24 (**a**, *lower panel*). H0R0 refers to no OGD normal control. Data are mean ± SD of at least three independent experiments performed in triplicate. For in vivo, rats were subjected to 0.5 ng, otherwise indicated, p22phox siRNA icv infusion immediately after 30-min MCA occlusion. At 24-h reperfusion, infarct volume (**d**), p22phox mRNA (**e**), protein oxidation (**f**), and apoptotic-related protein levels (**g**) in the ischemic brains were examined. Data are mean±SD, $n \geq 3$ otherwise indicated. ★★$P < 0.01$ versus control

protein oxidation, consistent with the notion that NOX-generated ROS plays a pivotal role in neuronal death and brain damage [4, 13, 51, 56]. In addition, levels of p-IκBα were not altered by p22phox siRNA, supporting the contention of the sequential PPAR-γ→NF-κB→p22phox→NOX→ROS signal transduction cascade (Fig. 10).

Albeit epidemiological studies showed mixed and sometimes contradictory relations between p22phox polymorphism and cerebrovascular disorders [57–60], the pathophysiological significance of PPAR-γ-p22phox signaling cascade under ischemic stress is further strengthened by recent reports that, besides Nox2, Nox1 and Nox4 genetic deletion also led to a

Fig. 9 Postischemic p22phox siRNA treatment reduces brain infarct and improves neurological deficits. Rats were subjected to 0.5 ng p22phox siRNA icv infusion right after 30-min MCA occlusion. At 1-week (1 W) reperfusion, infarct volume derived from T2-weighted MRI (**a**) and functional outcome based on Bederson's test (**b**) or elevated body swing test (**c**) were determined. Normal refers to sham control. Data are mean ± SD, $n \geq 3$ otherwise indicated. ★$P<0.05$ and ★★$P<0.01$ versus control
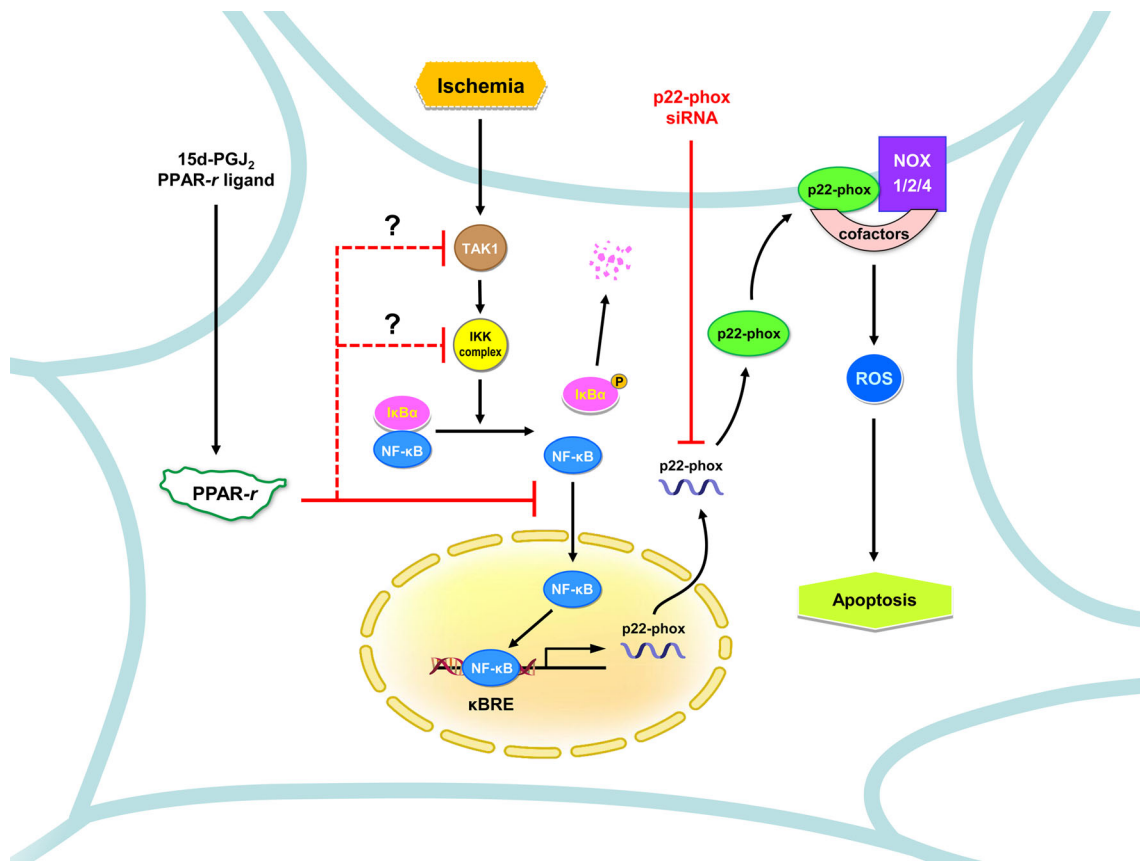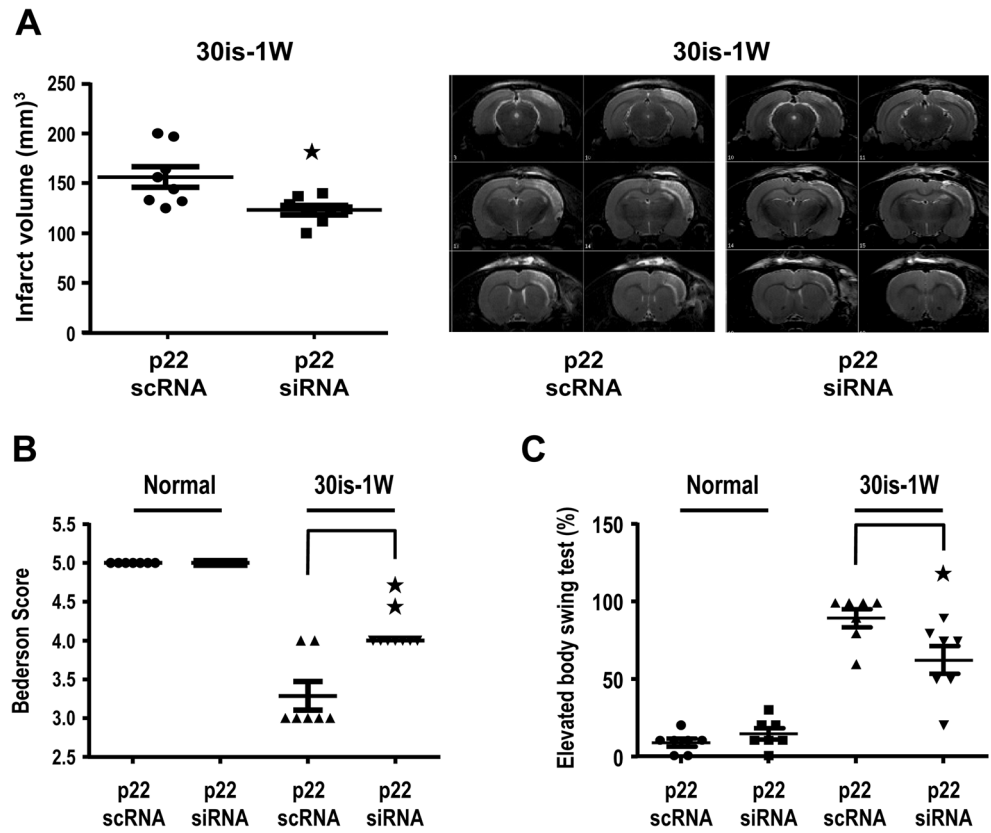

Fig. 10 A schematic drawing summarizes the beneficial effects of PPAR-γ protecting neurons against ischemic brain injury and potential studies in the future

smaller brain infarct after acute ischemic injury [20, 24, 25, 27]. Since these NOX isoforms all required p22phox for holoenzyme stabilization and maximum activation, attenuation of p22phox expression could simultaneously inhibit all three NOX isoforms.

In summary, it is well documented that PPAR-γ, a transcription factor, confers multifaceted neuroprotective actions. Here, we demonstrate a sequential neuroprotective signal cascade starting with 15d-PGJ$_2$ acting as a PPAR-γ agonist to attenuate NF-κB nuclear translocation to suppress NF-κB-driven p22phox transcription and subsequent NOX activation, ROS generation, ischemic neuronal death, and brain injury. This PPAR-γ→NF-κB→p22phox neuroprotective signaling cascade may be a new therapeutic target for reducing ischemic brain injury.

Conflict of Interest The authors declare that they have no conflict of interest.

References

1. Lloyd-Jones D, Adams RJ, Brown TM et al (2010) Heart disease and stroke statistics—2010 update: a report from the American Heart Association. Circulation 121:e46–e215
2. Hsieh FI, Lien LM, Chen ST et al (2010) Taiwan stroke registry investigators. Get with the guidelines-stroke performance indicators: surveillance of stroke care in the Taiwan stroke registry: get with the guidelines-stroke in Taiwan. Circulation 122(11):1116–1123
3. Chan PH (2001) Reactive oxygen radicals in signaling and damage in the ischemic brain. J Cereb Blood Flow Metab 21(1):2–14
4. Moskowitz MA, Lo EH, Iadecola C (2010) The science of stroke: mechanisms in search of treatments. Neuron 67:181–198
5. Chen H, Kim GS, Okami N, Narasimhan P, Chan PH (2011) NADPH oxidase is involved in post-ischemic brain inflammation. Neurobiol Dis 42:341–348
6. Kahles T, Brandes RP (2012) NADPH oxidases as therapeutic targets in ischemic stroke. Cell Mol Life Sci 69(14):2345–2363
7. Kleikers PW, Wingler K, Hermans JJ, Diebold I, Altenhöfer S, Radermacher KA, Janssen B, Görlach A, Schmidt HH (2012) NADPH oxidases as a source of oxidative stress and molecular target in ischemia/reperfusion injury. J Mol Med (Berl) 90(12):1391–1406
8. Tang XN, Cairns B, Kim JY, Yenari MA (2012) NADPH oxidase in stroke and cerebrovascular disease. Neurol Res 34(4):338–345
9. Brennan-Minnella AM, Won SJ, Swanson RA (2015) NADPH oxidase-2: linking glucose, acidosis, and excitotoxity in stroke. Antioxid Redox Signal 22(2):161–174
10. Bedard K, Krause KH (2007) The NOX family of ROS-generating NADPH oxidases: physiology and pathophysiology. Physiol Rev 87:245–313
11. Radermacher KA, Wingler K, Langhauser F, Altenhöfer S, Kleikers P, Hermans JJ, Hrabě de Angelis M, Kleinschnitz C, Schmidt HH (2013) Neuroprotection after stroke by targeting NOX4 as a source of oxidative stress. Antioxid Redox Signal 18(12):1418–1427
12. Brandes RP, Weissmann N, Schröder K (2014) Nox family NADPH oxidases: molecular mechanisms of activation. Free Radic Biol Med 76C:208–226
13. Chen H, Yoshioka H, Kim GS, Jung JE, Okami N, Sakata H, Maier CM, Narasimhan P, Goeders CE, Chan PH (2011) Oxidative stress in ischemic brain damage: mechanisms of cell death and potential molecular targets for neuroprotection. Antioxid Redox Signal 14(8):1505–1517
14. Beske PH, Jackson DA (2012) NADPH oxidase mediates the oxygen-glucose deprivation/reperfusion-induced increase in the tyrosine phosphorylation of the N-methyl-D-aspartate receptor NR2A subunit in retinoic acid differentiated SH-SY5Y Cells. J Mol Signal 7:15
15. He M, Zhang B, Wei X, Wang Z, Fan B, Du P, Zhang Y, Jian W, Chen L, Wang L, Fang H, Li X, Wang PA, Yi F (2013) HDAC4/5-HMGB1 signalling mediated by NADPH oxidase activity contributes to cerebral ischaemia/reperfusion injury. J Cell Mol Med 17:531–542
16. Hong H, Zeng JS, Kreulen DL, Kaufman DI, Chen AF (2006) Atorvastatin protects against cerebral infarction via inhibition of NADPH oxidase-derived superoxide in ischemic stroke. Am J Physiol Heart Circ Physiol 291:H2210–H2215
17. Tang LL, Ye K, Yang XF, Zheng JS (2007) Apocynin attenuates cerebral infarction after transient focal ischaemia in rats. J Int Med Res 35:517–522
18. Jackman KA, Miller AA, De Silva TM, Crack PJ, Drummond GR, Sobey CG (2009) Reduction of cerebral infarct volume by apocynin requires pretreatment and is absent in Nox2-deficient mice. Br J Pharmacol 156:680–688
19. Nagel S, Hadley G, Pfleger K, Grond-Ginsbach C, Buchan AM, Wagner S, Papadakis M (2012) Suppression of the inflammatory response by diphenyleneiodonium after transient focal cerebral ischemia. J Neurochem 123(Suppl 2):98–107
20. Walder CE, Green SP, Darbonne WC, Mathias J, Rae J, Dinauer MC, Curnutte JT, Thomas GR (1997) Ischemic stroke injury is reduced in mice lacking a functional NADPH oxidase. Stroke 28:2252–2258
21. Kahles T, Luedike P, Endres M, Galla HJ, Steinmetz H, Busse R, Neumann-Haefelin T, Brandes RP (2007) NADPH oxidase plays a central role in blood-brain barrier damage in experimental stroke. Stroke 38:3000–3006
22. Chen H, Song YS, Chan PH (2009) Inhibition of NADPH oxidase is neuroprotective after ischemia-reperfusion. J Cereb Blood Flow Metab 29:1262–1272
23. Suh SW, Shin BS, Ma H, Van Hoecke M, Brennan AM, Yenari MA, Swanson RA (2008) Glucose and NADPH oxidase drive neuronal superoxide formation in stroke. Ann Neurol 64:654–663
24. Kahles T, Kohnen A, Heumueller S, Rappert A, Bechmann I, Liebner S, Wittko IM, Neumann-Haefelin T, Steinmetz H, Schroeder K, Brandes RP (2010) NADPH oxidase Nox1 contributes to ischemic injury in experimental stroke in mice. Neurobiol Dis 40(1):185–192
25. Kleinschnitz C, Grund H, Wingler K, Armitage ME, Jones E, Mittal M et al (2010) Post-stroke inhibition of induced NADPH oxidase type 4 prevents oxidative stress and neurodegeneration. PLoS Biol. 8(9). doi:10.1371/journal.pbio.1000479
26. Drummond GR, Selemidis S, Griendling KK, Sobey CG (2011) Combating oxidative stress in vascular disease: NADPH oxidases as therapeutic targets. Nat Rev Drug Discov 10:453–471
27. Kahles T, Brandes RP (2013) Which NADPH oxidase isoform is relevant for ischemic stroke? The case for nox 2. Antioxid Redox Signal 18:1400–1417

28. Issemann I, Green S (1990) Activation of a member of the steroid hormone receptor superfamily by peroxisome proliferators. Nature 347:645–650

29. Chen YC, Wu JS, Tsai HD, Huang CY, Chen JJ, Sun GY, Lin TN (2012) Peroxisome proliferator-activated receptor gamma (PPAR-γ) and neurodegenerative disorders. Mol Neurobiol 46(1):114–124

30. Giaginis C, Tsourouflis G, Theocharis S (2008) Peroxisome proliferator-activated receptor-gamma (PPAR-gamma) ligands: novel pharmacological agents in the treatment of ischemia reperfusion injury. Curr Mol Med 8:562–579

31. Kapadia R, Yi JH, Vemuganti R (2008) Mechanisms of anti-inflammatory and neuroprotective actions of PPAR-gamma agonists. Front Biosci 13:1813–1826

32. Fong WH, Tsai HD, Chen YC, Wu JS, Lin TN (2010) Anti-apoptotic actions of PPAR-gamma against ischemic stroke. Mol Neurobiol 41:180–186

33. Zhao X, Strong R, Zhang J, Sun G, Tsien JZ, Cui Z, Grotta JC, Aronowski J (2009) Neuronal PPARgamma deficiency increases susceptibility to brain damage after cerebral ischemia. J Neurosci 29(19):6186–6195

34. Wu JS, Cheung WM, Tsai YS, Chen YT, Fong WH, Tsai HD, Chen YC, Liou JY, Shyue SK, Chen JJ, Chen YE, Maeda N, Wu KK, Lin TN (2009) Ligand-activated peroxisome proliferator-activated receptor-gamma protects against ischemic cerebral infarction and neuronal apoptosis by 14-3-3 epsilon upregulation. Circulation 119:1124–1134

35. Inoue I, Goto S, Matsunaga T, Nakajima T, Awata T, Hokari S, Komoda T, Katayama S (2001) The ligands/activators for peroxisome proliferator-activated receptor alpha (PPARalpha) and PPARgamma increase Cu2+, Zn2+-superoxide dismutase and decrease p22phox message expressions in primary endothelial cells. Metabolism 50:3–11

36. Nakamura T, Yamamoto E, Kataoka K, Yamashita T, Tokutomi Y, Dong YF, Matsuba S, Ogawa H, Kim-Mitsuyama S (2007) Pioglitazone exerts protective effects against stroke in stroke-prone spontaneously hypertensive rats, independently of blood pressure. Stroke 38:3016–3022

37. Hwang J, Kleinhenz DJ, Lassègue B, Griendling KK, Dikalov S, Hart CM (2005) Peroxisome proliferator-activated receptor-gamma ligands regulate endothelial membrane superoxide production. Am J Physiol Cell Physiol 288:C899–C905

38. Wu JS, Tsai HD, Huang CY, Chen JJ, Lin TN (2014) 15-Deoxy-$\Delta^{12,14}$-PGJ$_2$, by activating peroxisome proliferator-activated receptor-gamma, suppresses p22phox transcription to protect brain endothelial cells against hypoxia-induced apoptosis. Mol Neurobiol 50(1):221–238

39. Ceolotto G, Gallo A, Papparella I, Franco L, Murphy E, Iori E, Pagnin E, Fadini GP, Albiero M, Semplicini A, Avogaro A (2007) Rosiglitazone reduces glucose-induced oxidative stress mediated by NAD(P)H oxidase via AMPK-dependent mechanism. Arterioscler Thromb Vasc Biol 27:2627–2633

40. Potenza MA, Gagliardi S, De Benedictis L, Zigrino A, Tiravanti E, Colantuono G, Federici A, Lorusso L, Benagiano V, Quon MJ, Montagnani M (2009) Treatment of spontaneously hypertensive rats with rosiglitazone ameliorates cardiovascular pathophysiology via antioxidant mechanisms in the vasculature. Am J Physiol Endocrinol Metab 297:E685–E694

41. Schock SC, Xu J, Duquette PM, Qin Z, Lewandowski AJ, Rai PS, Thompson CS, Seifert EL, Harper ME, Chen HH (2008) Rescue of neurons from ischemic injury by peroxisome proliferator-activated receptor-gamma requires a novel essential cofactor LMO4. J Neurosci 28(47):12433–12444

42. Lin TN, Cheung WM, Wu JS, Chen JJ, Lin H, Chen JJ, Liou JY, Shyue SK, Wu KK (2006) 15d-Prostaglandin J2 protects brain from

ischemia-reperfusion injury. Arterioscler Thromb Vasc Biol 26:481–487

43. Wu JS, Lin TN, Wu KK (2009) Rosiglitazone and PPAR-γ overexpression protect mitochondrial membrane and prevent mitochondria-mediated apoptosis by upregulating anti-apoptotic Bcl-2 family proteins. J Cell Physiol 220(1):58–71

44. Huang CY, Chen JJ, Wu JS, Tsai HD, Lin H, Yan YT, Hsu CY, Ho YS, Lin TN (2015) Novel link of anti-apoptotic ATF3 with pro-apoptotic CTMP in the ischemic brain. Mol Neurobiol 51(2):543–557

45. Goldberg MP, Choi DW (1993) Combined oxygen and glucose deprivation in cortical cell culture: calcium-dependent and calcium-independent mechanisms of neuronal injury. J Neurosci 13:3510–3524

46. Lin H, Lin TN, Cheung WM, Nian GM, Tseng PH, Chen SF, Chen JJ, Shyue SK, Liou JY, Wu CW, Wu KK (2002) Cyclooxygenase-1 and bicistronic cyclooxygenase-1/prostacyclin synthase gene transfer protect against ischemic cerebral infarction. Circulation 105:1962–1969

47. Lin TN, He YY, Wu G, Khan M, Hsu CY (1993) Effect of brain edema on infarct volume in a focal cerebral ischemia model in rats. Stroke 24:117–121

48. Bederson JB, Pitts LH, Tsuji M, Nishimura MC, Davis RL, Bartkowski H (1986) Rat middle cerebral artery occlusion: evaluation of the model and development of a neurologic examination. Stroke 17:472–476

49. Borlongan CV, Cahill DW, Sanberg PR (1995) Locomotor and passive avoidance deficits following occlusion of the middle cerebral artery. Physiol Behav 58(5):909–917

50. Lin TN, Sun SW, Cheung WM, Li F, Chang C (2002) Dynamic changes in cerebral blood flow and angiogenesis after transient focal cerebral ischemia in rats. Evaluation with serial magnetic resonance imaging. Stroke 33:2985–2991

51. Abramov AY, Scorziello A, Duchen MR (2007) Three distinct mechanisms generate oxygen free radicals in neurons and contribute to cell death during anoxia and reoxygenation. J Neurosci 27(5):1129–1138

52. Shimazu T, Inoue I, Araki N, Asano Y, Sawada M, Furuya D, Nagoya H, Greenberg JH (2005) A peroxisome proliferator-activated receptor-gamma agonist reduces infarct size in transient but not in permanent ischemia. Stroke 36(2):353–359

53. Hashimoto R, Umemoto S, Guo F, Umeji K, Itoh S, Kishi H, Kobayashi S, Matsuzaki M (2010) Nifedipine activates PPARgamma and exerts antioxidative action through Cu/ZnSOD independent of blood-pressure lowering in SHRSP. J Atheroscler Thromb 17(8):785–795

54. Zhang HL, Xu M, Wei C, Qin AP, Liu CF, Hong LZ, Zhao XY, Liu J, Qin ZH (2011) Neuroprotective effects of pioglitazone in a rat model of permanent focal cerebral ischemia are associated with peroxisome proliferator-activated receptor gamma-mediated suppression of nuclear factor-κB signaling pathway. Neuroscience 176:381–395

55. Skaug B, Jiang X, Chen ZJ (2009) The role of ubiquitin in NF-kappaB regulatory pathways. Annu Rev Biochem 78:769–796

56. Brennan AM, Suh SW, Won SJ, Narasimhan P, Kauppinen TM, Lee H, Edling Y, Chan PH, Swanson RA (2009) NADPH oxidase is the primary source of superoxide induced by NMDA receptor activation. Nat Neurosci 12(7):857–863

57. Ito D, Murata M, Watanabe K, Yoshida T, Saito I et al (2000) C242T polymorphism of NADPH oxidase p22 PHOX gene and ischemic cerebrovascular disease in the Japanese population. Stroke 31:936–939

58. Kuroda J, Kitazono T, Ago T, Ninomiya T, Ooboshi H et al (2007) NAD(P)H oxidase p22phox C242T polymorphism and ischemic stroke in Japan: the Fukuoka Stroke Registry and the Hisayama study. Eur J Neurol 14:1091–1097

59. Niemiec P, Zak I, Emich-Widera E, Balcerzyk A, Kopyta I et al (2010) The C242T polymorphism of the gene encoding cytochrome b-245 alpha is not associated with paediatric ischaemic stroke: family-based and case-control study. Neurol Neurochir Pol 44: 453–458

60. Li BH, Zhang LL, Zhang BB, Yin YW, Dai LM, Pi Y, Guo L, Gao CY, Fang CQ, Wang JZ, Li JC (2013) Association between NADP H oxidase p22(phox) C242T polymorphism and ischemic cerebro-vascular disease: a meta-analysis. PLoS One 8(2), e56478. doi:10. 1371/journal.pone.0056478